Prediction of microporosity in Al-Si castings in low pressure permanent mould casting using criteria functions

Shang, L. H.; Paray, F.; Gruzleski, J. E.; Bergeron, S.; Mercadante, C.; Loong, C. A.

Publisher's version / Version de l'éditeur:
https://doi.org/10.1179/136404604225020650
International Journal of Cast Metals Research, 17, 4, pp. 193-200, 2004-12-20

Prediction of microporosity in Al–Si castings in low pressure permanent mould casting using criteria functions

L. H. Shang[1]*, F. Paray[1], J. E. Gruzleski[1], S. Bergeron[2]†, C. Mercadante[2]‡ and C. A. Loong[2]

[1]*Department of Mining, Metals and Materials Engineering, McGill University, M.H. Wong Building, Room 2160, 3160 University Street, Montreal, Que., H3A 2B2*
[2]*Industrial Materials Institute, National Research Council Canada, Boucherville, Que., Canada J4B 6Y4*

Microporosity, a serious defect in Al–Si based castings, severely prevents their widespread applications in many critical conditions. The use of criteria functions to predict quantitatively microporosity level holds promise. To date, an ideal criteria function has yet to be obtained. In the present work, microporosity distribution in three prominently used hypoeutectic Al–Si alloys (319, 356 and 332) was investigated. The prediction effectiveness of single solidification parameter and existing criteria functions was evaluated by correlating thermal data of simulation studies to experimentally obtained microporosity values. Two new criteria functions are proposed based on experimental observation and multivariable regression analysis. The results indicate that thermal parameter-based criteria functions may be used to predict the microporosity in Al–Si castings but have their limitations. A general criteria function $t_f^{1.18}$ $V_s^{1.13}$ (t_f, local solidification time; V_s, solidification velocity) can be applied to predict microporosity for the family of hypoeutectic Al–Si casting alloys within a certain error. IJCMR/522

 Manuscript received 24 June 2004; accepted 23 July 2004.

Keywords: Microporosity; Prediction; Criteria functions; Al–Si castings

Introduction

Microporosity in Al–Si castings is one of the most detrimental defects responsible for high scrap loss in the production of commercial castings and severely prevents their widespread uses in many critical load-bearing conditions. The damaging effects of microporosity are lack of pressure tightness, limited strength, variable fracture toughness and notable reduction in ductility as well as lower fatigue resistance.[1–4] Prediction of microporosity amounts in castings is significant from both a practical and a scientific point of view. The formation of microporosity during solidification is a very complicated process, involving heat, mass and fluid flow. It has been basically accepted that microporosity in cast aluminium silicon alloys is a result of two main factors: hydrogen rejection as a result of a drastic reduction in the solubility from liquid to solid phase, and/or the volume contraction coupled with poor interdendritic feeding during mushy zone solidification.[5–8]

There have been numerous studies on porosity prediction in cast aluminium alloys since the 1950s. Most of these focus on establishing various relationships between the casting conditions (alloy composition, solidification parameters, hydrogen content, treatment of liquid metal, use of risers and chills) and the porosity level found in castings (per cent porosity, size or shape of porosity). The methods used vary from simple criteria functions based on experimental studies to complicated continuum models considering the fluid flow coupled with several conservation and continuity equations, as well as nucleation and growth of hydrogen pores.[9–13] Criteria functions consist of solidification parameters (e.g. thermal gradient G, cooling rate R, solidification time t_f and solidification velocity V_s), by which the per cent porosity can be calculated directly from the derived mathematical equation. By comparison, the continuum models based on formation mechanisms are currently too computationally complicated to be used in industrial practice. Since solidification parameters can be simulated by computer modelling, the criteria function method seems to be a practical way for casting producers to predict an appropriate solidification condition necessary to control porosity under a required critical level. During the past few decades, a number of porosity criteria functions were proposed under different casting conditions (Table 1).[14–24] Among all of these, there is a noticeable absence of sufficient research on the prediction of microporosity in a variety of hypoeutectic Al–Si alloys commonly used in the automotive industry. In addition, little attention has been paid to microporosity prediction under low pressure permanent mould (LPPM) casting conditions. As a result, there is a lack of understanding of whether the existing

*Corresponding author, email lihong.shang@mail.mcgill.ca
†Present address: styl & tech Inc., complex shape engineering, 3700 rue du Campanile, Sainte-Foy, Que., Canada G1X 4G6.
‡Present address: Chemistry Department, Faculty of Science and General Studies, Vanier College, 821 Ste Croix, St. Laurent, Que., Canada H4L 3X9.

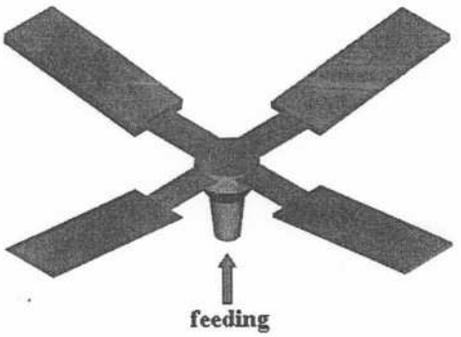

1 Schematic diagram of plate samples with four different thicknesses

criteria functions can be used for the quantitative prediction of the amount of microporosity in commonly used Al–Si castings formed by the LPPM process.

The work presented in this paper is part of a project conducted by McGill University and its partners on the use of criteria functions to predict microporosity levels quantitatively in prominently used Al–Si alloys in the automotive industry. The characterisation of the castings is investigated in terms of microporosity distributions and thermal parameters under LPPM casting conditions. Attempts to correlate the microporosity to a single thermal parameter and existing criteria functions in an empirical way are presented and evaluated. Two new criteria functions are developed by experimental observation and multivariable regression analysis. The degree of fit and the limitations of the criteria function method are also discussed.

Experimental

Samples

A die was designed to produce four plate samples with different thicknesses as described in a previous study on thermal analysis.[25,26] The plate castings are shown schematically in Fig. 1. The four thicknesses are 3·2 mm (1/8″), 6·4 mm (1/4″), 12·7 mm (1/2″) and 19·1 mm (3/4″). This geometry was selected for two main reasons: the simple plate shape is a basic form found in castings, and it is readily amenable to thermal modelling. The length and width of the plates were 279·4 mm (11″) and 101·6 mm (4″), respectively, and the sizes of the gates were 50·8 mm (2″) in width with a thickness ratio of 2 : 3 between the gates and the plates.

Alloys and production of castings

Commercial aluminium–silicon alloys 319, 356 and 332 were used. The chemical compositions of the alloys are given in Table 2. All alloys were modified with 180 ppm strontium. Castings were produced in an industrial environment using a low pressure permanent mould casting machine located at Grenville Castings Ltd in Perth, Ont. A $2{\cdot}1 \times 10^4$ Pa (3 psi) gauge pressure was used to ensure that the molten metal rose steadily up through the feed tube into the die. The casting cycle time consists of three portions: cast or pressure time, cooling time and open time. The related process parameters are listed in Table 3, and the crucible melt temperatures are given in Table 4. On average, producing a casting (four plate samples) took 3·2–3·5 min. The hydrogen level of the melt was determined by a modified Straube-Pfeiffer test developed at McGill to give a quantitative value of the hydrogen content.[27,28] The gas level in the melt (normal gas level of the as melted metal) was estimated to be in the range of 0·20–0·30 mL H_2/100 g Al for all the alloys.

Microporosity determination

The microporosity volume percentage was determined by density measurement calculated by Archimedes's principle. For each alloy, several plate castings produced in the steady state were randomly selected and radiographed in order to obtain a general idea of soundness. Each plate was sectioned into three parts along the length, referred to as middle, left and right slices. Each slice was then cut into 19 small rectangular blocks with dimensions of

Table 2 Chemical compositions of alloys

Alloy	Si, %	Fe, %	Cu, %	Mn, %	Mg, %	Zn, %	Ti, %	Al, %
319	6·25	0·42	3·62	0·28	0·06	0·53	0·16	Balance
356	7·30	0·11	0·06	0·06	0·34	0·01	0·014	Balance
332	9·33	0·19	2·87	0·03	1·06	0·10	0·12	Balance

Table 1 Criteria functions for porosity prediction surveyed from literature

No.	Criteria function	Reference	Year	Alloy	Casting process
1	Thermal gradient: G	14	1959	Al–7Mg alloy	Sand
2	Solidification time: t_f	15	1973	Al–Cu–Si (LM4)	Sand
3	Feeding index (FI): G/t_f	15	1973	Al–Cu–Si (LM4)	Sand
4	Solidus velocity: V_s	16	1975	Steel; cast iron; Al, Mg and Cu alloys	Sand
5	Niyama: $G/R^{1/2}$; G: thermal gradient; R: cooling rate	17	1982	Steel	Sand
6	LCC: $G \cdot t_f^{2/3}/V_s$	18	1990	Al–7Si–0·3Mg; $H_2 < 0{\cdot}01$ mL/100 g Al	Sand
7	Feeding efficiency: $G/(V_s \cdot t_f^{1{\cdot}1})$	19	1994	A201 Al alloy	Sand
8	$G^{-0{\cdot}474} \cdot V_s^{-0{\cdot}317}$	20,21	1994	A356 Al alloy	Sand
	KCL: $G^{0{\cdot}4}/V_s^{1{\cdot}6}$	22	1995	Al–4·5Cu alloy	Graphite tube directional solidification
9	$G^{0{\cdot}38}/V_s^{1{\cdot}62}$	23	1996	Al–7Si–0·3Mg	Sand
10	$G/(R^{1/2} \cdot t_f^{3n})$; $n = 3{\cdot}4333H_2^{0{\cdot}9807}$	24	2000	A356 Al alloy	Lost foam

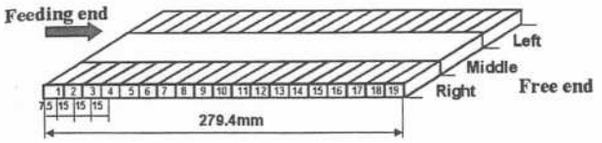

2 Schematic diagram of small blocks used for porosity determination

$33 \times 15 \times$ (plate-thickness) mm^3 (Fig. 2). The density and per cent microporosity of the small blocks were calculated by the following equations

$$D_M = \frac{M_a}{(M_a - M_w)} \times D_w, \; \%P = \frac{D_T - D_M}{D_T} \times 100$$

where M_a is the sample mass in air (kg), M_w is the sample mass in water (kg), D_M is the measured density of the small block sample (kg m^{-3}), D_T is the theoretical density of the alloy (kg m^{-3}), D_w is the density of water (kg m^{-3}), and P is the volume percentage of microporosity (%).

The theoretical densities of the three alloys were obtained using sound disc samples cast in a copper mould. The values for 319, 356 and 332 alloys were $2{\cdot}788 \times 10^3$, $2{\cdot}678 \times 10^3$ and $2{\cdot}725 \times 10^3$ kg m^{-3}, respectively.

From the individual value for each block, a microporosity distribution map of the entire plate could be obtained.

Simulation for thermal parameters

The simulation package used for this project was CASTVIEW developed at the Industrial Materials Institute at Boucherville, Que. The simulation process was performed using a SGI Origin 2000 computer composed of 16 processors with a total of 8 Gigabytes of RAM at 250 MHz IP27. By computer modelling of filling, heat transfer and solidification, the thermal conditions within a casting at any location could be obtained. The locations chosen were those where the per cent porosity was determined experimentally. At each node (sample) point, four kinds of thermal data were calculated: t_f, local solidification time, s; R, cooling rate at the solidus, K s^{-1}; G, thermal gradient at the solidus, K mm^{-1}; V_s, solidification velocity, mm s^{-1}.

The model data were validated by comparison to temperature measurements taken on the castings during solidification.

Results and discussion

Microporosity distribution in plate samples

Microporosity, defined as micrometre scale cavities (10–300 μm),[29] is the focus in criteria function development. Since some massive macroshrinkage was found in the middle slices of the plate castings, only the side slices were used for the data source. In addition, a few porosity values greater than 2% which relate to open macroshrinkage pores were removed from the data set.

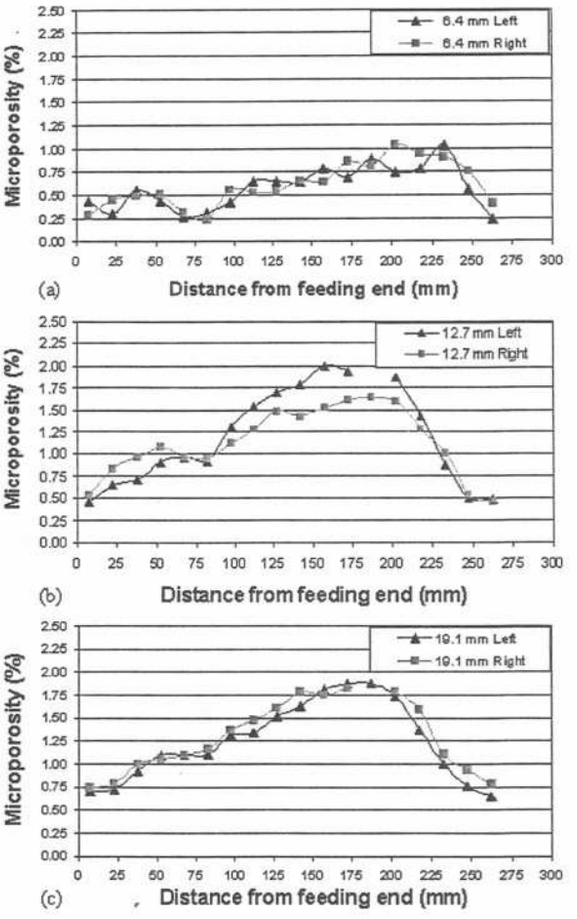

a 6·4 mm thickness; *b* 12·7 mm thickness; *c* 19·1 mm thickness

3 Typical microporosity distribution in different thickness plates for 319 alloy

The microporosity distributions in three plate thicknesses (6·4, 12·7 and 19·1 mm) for all three alloys (319, 356 and 332) were investigated. The amount of microporosity related to the distance from the feeding end of the plate castings was plotted as shown in Fig. 3. Each point on the graph represents the average calculated from four randomly selected samples. Figure 3 compares the microporosity distributions in different thickness plates for 319 alloy. The results indicate that the thicker the cross-section of the sample, the higher the microporosity level. This is consistent with the expectation that in the thicker plates the lower cooling rate and longer solidification time lead to a greater amount of microporosity. In addition, it is noted that the microporosity is much greater in the middle than at the two ends because of

Table 3 LPPM process parameters for casting samples

Alloys	Pressure time, s	Cooling time, s	Open time, s	Cycle time, s
319	90	90	31	211
356	96	80	30	206
332	80	80	31	191

Table 4 Metal temperature (°C) in crucible

Alloys	319 with Sr	356 with Sr	332 with Sr
Temperature (°C)	746	745	721

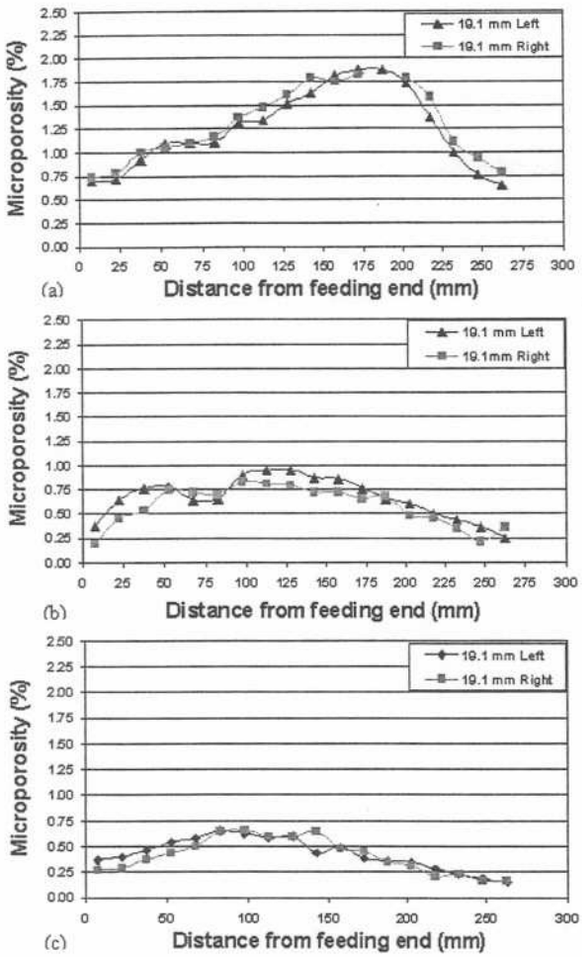

a 319 alloy; *b* 356 alloy; *c* 332 alloy

4 Typical microporosity distribution in 19·1 mm thickness plates for different alloys

the late solidification in the middle zone. Moreover, it also can be observed that the microporosity distributions for the left and right side slices are not identical, although they are of the same general form. The difference is a result of the slightly different solidification conditions caused by the adjacent plate, which may be thicker or thinner depending on location. As a result, the heat flux during solidification is different for the left and right sides of each plate.

Figure 4 illustrates the microporosity distribution in the same thickness plates (19·1 mm) for three different alloys (319, 356 and 332). The effect of alloy composition on the formation of microporosity is clearly demonstrated. The higher the silicon content, the lower the microporosity displayed. For Al–Si alloys, with the increase in the weight percentage of silicon (319 alloy: 6·25 Si%, 356 alloy: 7·30 Si% and 332 alloy: 9·33 Si%), the freezing range and the amount of primary α-Al dendrites will decrease. Thus, the dendrite network will form later, and the feeding resistance through the interdendritic space is reduced resulting in an increased feeding ability.

Thermal parameters from simulation

Thermal parameters specify the solidification conditions. Four kinds of basic thermal data, including

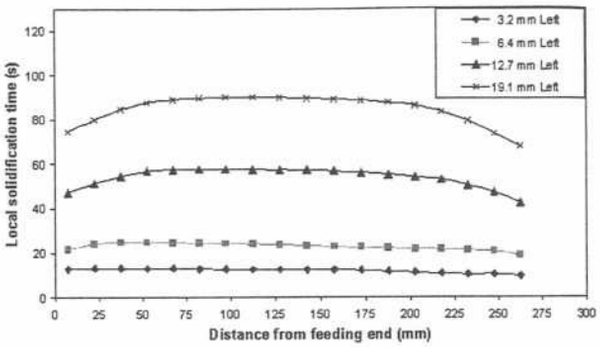

5 Example of simulated thermal data: local solidification time (t_f) in different thickness plates for 356 alloy

local solidification time (t_f), thermal gradient at the solidus (G), cooling rate at the solidus (R), and solidification velocity (V_s), were simulated corresponding to different locations in the plate castings. A very large number of thermal data were obtained and only some typical results of the local solidification time (t_f) in four different thickness samples for 356 alloy will be discussed as an example here. Local solidification time versus specific location (distance from feeding end) is shown in Fig. 5. Signs of decreasing local solidification time can be first observed at the two ends of the plates whereas the centre remains at higher values. This observation becomes more pronounced with the thicker plates (12·7 and 19·1 mm) because of the larger quantity of metal involved. Meanwhile the thinnest plates (3·2 mm) appear to have a uniform distribution as a result of relatively equal cooling rate, and of course the thicker the plates, the longer the local solidification time since more liquid metal needs to solidify.

Evaluation of effectiveness of single thermal parameter and existing criteria functions

The method of correlation analysis is displayed in Table 5. The dependent variable is the per cent microporosity, and independent variables are the various porosity criteria. In order to find the best-fit predictive equation, five regression models for correlation analysis were used: linear, logarithmic, polynomial, power and exponential models. The analysis step is illustrated in Fig. 6. The correlation analysis begins with a single alloy using the data of three different thicknesses, respectively, to investigate the effect of the geometry factor on the microporosity level. Since a real casting always consists of different cross-sections, the data combining the three thicknesses are then used to evaluate the effectiveness for microporosity prediction in a more real casting. Next, the data combining three alloys with all of the thicknesses are used to survey whether there is a general criteria function able to predict the microporosity level for the family of hypoeutectic Al–Si castings.

A statistical term, the coefficient of determination denoted by r^2, provides a measure of the goodness of fit for the estimated regression equation. The

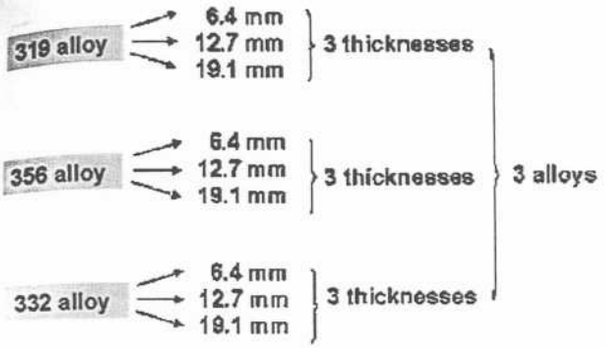

6 Schematic illustration of steps for correlation analysis

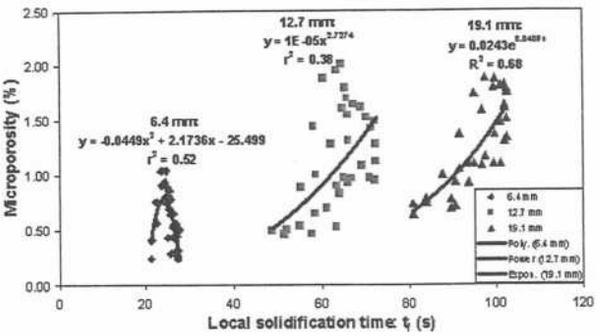

7 Example of evaluation of single parameter – local solidification time (t_f) for 319 alloy with three different thicknesses, respectively, $P(\%) = f(t_f)$

coefficient of determination can have values between zero and one[30]

$$r^2 = \frac{\sum(\hat{y}_i - \bar{y})^2}{\sum(y_i - \bar{y})^2}$$

where y_i is the measured value of microporosity (%), $\hat{y}_i$ is the estimated value of microporosity (%) and $\bar{y}$ is the mean value for the microporosity (%). The r^2 value indicates the percentage of variation of the dependent variable which can be explained by using the predicting equation.

A value of $r^2 = 1$ indicates that the predicting equation can account for all variation in microporosity. A value of $r^2 = 0{\cdot}60$ indicates that 60% of the variation in microporosity can be explained by the predicting equation with related porosity criteria as the independent variable. Therefore, the greater the r^2 value, the better the effectiveness of prediction. As a practical matter, for the typical data found in social sciences, values of r^2 as low as 0·25 are considered useful, whereas r^2 values of 0·60 or greater are rational in physical and life sciences. It is the authors' opinion that for predicting microporosity in castings, values of r^2 greater than 0·25 can be considered indicative, whereas values around 0·50 indicate that the criteria function may be used for prediction.

The evaluation results of Table 6 show the prediction effectiveness for the simple plates with a certain thickness. Some r^2 values of around 0·50 or greater mean that the related porosity criteria may be used to predict microporosity in the castings with a uniform cross-section, and there will be some estimation errors. As can be seen in Table 6, the correlation results associated with the 19·1 mm (3/4″) thickness samples are almost always higher than those of 6·4 mm (1/4″) and 12·7 mm (1/2″) samples, no matter the porosity criteria or alloy type. Figure 7 as an illustration also demonstrates that different predictive equation models and r^2 values correspond to different thickness plates.

Table 7 gives the results of the evaluation for microporosity prediction in the single Al–Si alloys and the family of hypoeutectic alloys based on the data for all three thicknesses considered together. Although none of the values of r^2 is greater than 0·50 for the three kinds of single alloys, the single thermal parameter does have some impact on the microporosity amount in certain alloys. This effect is clearly suggested by some values, such as t_f and G (0·47) as well as R (0·38) for 319 alloy, and G (0·42) for 356 alloy. When the data for the entire hypoeutectic alloy family is considered, the highest value of r^2 is only 0·17. This result indicates that the single thermal parameter and existing criteria functions cannot be simply used as a general criterion to predict microporosity for the family of hypoeutectic Al–Si casting alloys.

New or improved criteria functions

New improved criteria function – $t_f/(0{\cdot}5L)$

Based on the above results and discussion of the comprehensive evaluation, the local solidification time (t_f) is always a major factor in the prediction of microporosity for different Al–Si alloys as in the thickness of the solidified part. A new criteria function has been proposed in the form of $t_f/(0{\cdot}5L)$

Table 5 Basic method for correlation analysis

Dependent variable (y) (measured)	Independent variables (x) (simulated)	
Microporosity, P, %	Single parameter	Local solidification time: t_f
		Cooling rate: R
		Thermal gradient: G
		Solidification velocity: V_s
	Existing criteria function	Niyama: $GR^{-1/2}$
		LCC: $Gt_f^{2/3} \cdot V_s^{-1}$
Regression models for correlation analysis	Linear	$y = ax + b$
	Logarithmic	$y = a \ln x + b$
	Polynomial	$y = ax^2 + bx + c$
	Power	$y = ax^b$
	Exponential	$y = ae^{bx}$

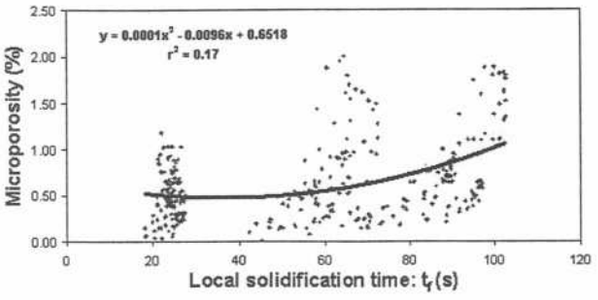

8 Correlation between microporosity and local solidification time (t_f) for three Al–Si alloys (319, 356 and 332), $P(\%) = f(t_f)$

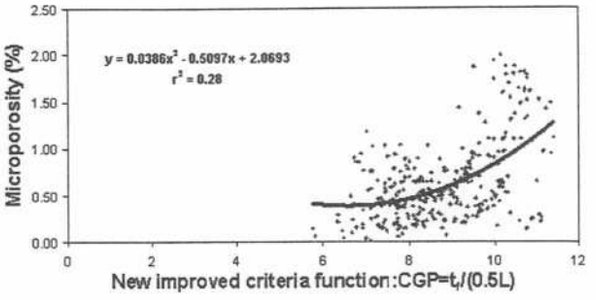

9 Correlation between microporosity and CGP (t_f) for three Al–Si alloys (319, 356 and 332), $P(\%) = f(\text{CGP}) = [(t_f/0{\cdot}5L)]$

known as the CGP factor, where L is the thickness of castings. Figures 8 and 9 compare the data distribution of two criteria, t_f and CGP. As can be observed from the figures, the data are more scattered for the single factor (t_f) than that for CGP which combines the two parameters, t_f and L. The low r^2 value of 0·28 in Fig. 9 stems from the fact that data from the 6·4 mm plates always shows a poorer correlation than data from thicker plates. An example of the application of the CGP criterion to a thicker 19·1 mm plate is shown in Fig. 10 where a good correlation is obtained between measured and predicted values.

New general criteria function for hypoeutectic Al–Si castings

The method of multivariable regression analysis was used to develop a general criteria function to predict microporosity for the family of hypoeutectic Al–Si castings. In regression models, the dependent variable is the per cent microporosity, and the independent variables are a series of thermal parameters as defined in the previous sections. Different combinations of parameters are displayed in Table 8. The commercial statistics software package SAS 8·2 was used for the multiple regression analysis.

Table 6 Evaluation of single parameter and existing criteria functions for single Al–Si alloys with different thicknesses

			Coefficient of determination: r^2		
No.	Porosity criteria	Sample thickness	319-Sr	356-Sr	332-Sr
1	t_f	6·4 mm (¼″)	0·52	0·32	0·09
		12·7 mm (⅜″)	0·38	0·49	0·18
		19·1 mm (¾″)	0·68	0·29	0·77
2	R	6·4 mm (¼″)	0·11	0·27	0·05
		12·7 mm (⅜″)	0·01	0·52	0·14
		19·1 mm (¾″)	0·33	0·52	0·66
3	G	6·4 mm (¼″)	0·08	0·29	0·03
		12·7 mm (⅜″)	0·22	0·70	0·11
		19·1 mm (¾″)	0·28	0·76	0·73
4	V_s	6·4 mm (¼″)	0·36	0·18	0·04
		12·7 mm (⅜″)	0·09	0·36	0·09
		19·1 mm (¾″)	0·53	0·32	0·26
5	Niyama	6·4 mm (¼″)	0·16	0·27	0·04
		12·7 mm (⅜″)	0·21	0·67	0·04
		19·1 mm (¾″)	0·43	0·69	0·48
6	LCC	6·4 mm (¼″)	0·31	0·24	0·03
		12·7 mm (⅜″)	0·16	0·57	0·01
		19·1 mm (¾″)	0·41	0·57	0·31

Table 7 Evaluation of single parameter and existing criteria functions for hypoeutectic Al–Si alloys

		Coefficient of determination: r^2			
No.	Porosity criteria	319 (three thicknesses)	356 (three thicknesses)	332 (three thicknesses)	319, 356 and 332 alloys (three thicknesses)
1	t_f	0·47	0·16	0·24	0·17
2	R	0·38	0·13	0·01	0·05
3	G	0·47	0·42	0·05	0·02
4	V_s	0·21	0·04	0·12	0·08
5	Niyama	0·02	0·11	0·07	0·14
6	LCC	0·24	0·04	0·03	0·09

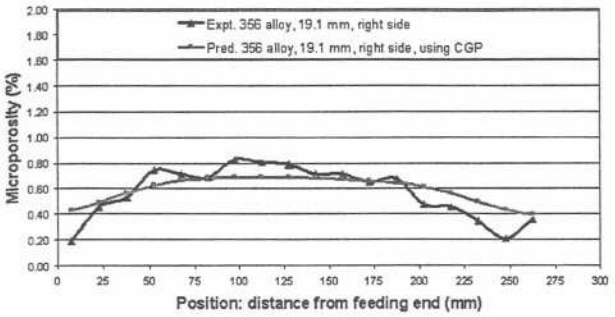

10 Example for prediction of microporosity using CGP [(t_f/0·5L)] in 19·1 mm thickness plate of 356 alloy

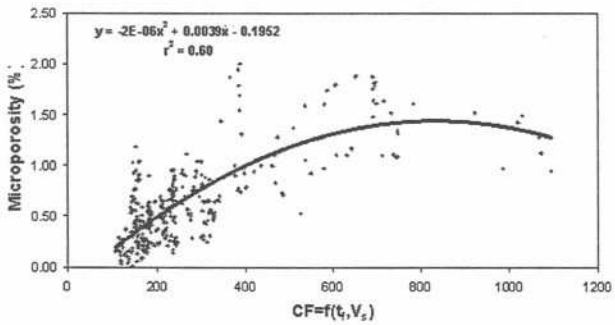

11 Predicting microporosity in hypoeutectic Al–Si castings (319, 356 and 332) using new general criteria function, $P(\%) = f(t_f,\ V_s) = f(t_f^{1.18} V_s^{1.13})$

The results indicate that the parameter combination of $t_f^{1.18} V_s^{1.13}$ is an effective new criteria function since it presents the highest r^2 value and is a simple form with only two parameters. Figure 11 shows a much more concentrated data distribution ($r^2 = 0.60$) than does Fig. 8 ($r^2 = 0.17$), and a stronger correlation than in Fig. 9 ($r^2 = 0.28$) for CGP function. The value of r^2 is increased by 43%, compared with the previous best result of 0·17 from the evaluation for single parameter and existing criteria functions.

A prediction using this new criteria function is shown in Fig. 12. The values expressed by square symbols indicate the measured microporosity values from four selected samples, which were used for the regression analysis. The values with triangular symbols are the predicted microporosity values calculated from the predicting equation. As can be noted, the average error between them is less than 0·2% microporosity. The values shown as open circle symbols are the per cent microporosity measured from a sample that was randomly selected and not used for the initial regression analysis. In order to examine the prediction error of using the new general criteria function, the statistical term, standard error of the estimate (e) is used. This is the square root of the average squared error of the prediction. Table 9 shows the results related to 356 alloy. The thicker samples (19·1 and 12·7 mm thickness) present a lower error (0·17), whereas the error is larger (0·32) for the thinner plates (6·4 mm). The average error is 0·23 for the entire 356 alloy data set.

Table 8 Multivariable regression models for development of new criteria function

No.	Regression model	No.	Regression model
1	$P = a \cdot t_f^b \cdot L^c$	6	$P = a \cdot t_f^b$
2	$P = a \cdot t_f^b \cdot R^c \cdot L^d$	7	$P = a \cdot t_f^b \cdot R^c$
3	$P = a \cdot t_f^b \cdot G^c \cdot L^d$	8	$P = a \cdot t_f^b \cdot G^c$
4	$P = a \cdot t_f^b \cdot V_s^c \cdot L^d$	9	$P = a \cdot t_f^b \cdot V_s^c$
5	$P = a \cdot t_f^b \cdot G^c \cdot R^d \cdot L^e$	10	$P = a \cdot t_f^b \cdot G^c \cdot R^d$

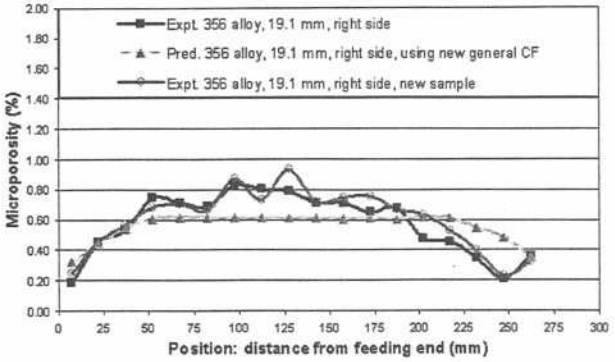

12 Evaluation of new general criteria function ($t_f^{1.18} V_s^{1.13}$) for predicting microporosity in 19·1 mm thickness plate of 356 alloy

It should be emphasised that criteria functions based on experimental studies only consider the thermal parameters. The effects of other significant factors on the formation of microporosity, such as hydrogen precipitation, alloy type and treatment of liquid metal, are neglected. This inevitably causes two inherent limitations for microporosity prediction in Al–Si castings, the predicting error and the required specific solidification condition under which the criteria function is obtained. However, the criteria function method provides a simple way for the general prediction of microporosity in Al–Si castings. Criteria functions can be a useful guide for casting producers to establish a suitable solidification condition to maintain the microporosity under a required critical level.

Conclusions

1. Alloy type is an important factor in determining the inherent microporosity amount in Al–Si castings. The lower the silicon content, the greater the tendency for microporosity formation.

2. The thermal parameters associated with the solidification process have a strong impact on the formation of the microporosity in Al–Si alloys.

Table 9 Standard error of estimate for microporosity prediction in 356 alloy

Thickness	e^*: Standard error of the estimate
6·4 mm (¼″)	0·32
12·7 mm (⅞″)	0·17
19·1 mm (¾″)	0·17
All data	0·23

*$e = \sqrt{\frac{SSE}{(n-p-1)}} = \sqrt{\frac{\sum (y_i - \hat{y})^2}{(n-p-1)}}$, where SSE: sum of residual squares owing to error, $p = 2$: number of independent variables, n: number of statistical records, y_i: measured microporosity value, %, $\hat{y}$: estimated microporosity value, %.

The local solidification time, which is related to casting thickness, is particularly important.

3. Thermal parameter-based criteria functions may be used to predict the microporosity in Al–Si castings, but have their limitations.

4. Two new criteria functions have been developed, which yield much better predicting results than the existing criteria functions. Of those two, the general criteria function $t_f^{1{\cdot}18} V_s^{1{\cdot}13}$ can be used to predict microporosity with less error than does the CGP function.

Acknowledgements

The authors wish to acknowledge the financial and technical support of all six partners in this project: Natural Sciences and Engineering Research Council of Canada (NSERC), Grenville Castings Ltd (Ont.), Timminco Metals a division of Timminco Ltd (Haley, Ont.), the Centre de Métallurgie du Cégep de Trois Rivières (Trois Rivières, Québéc), the Institute of Industrial Materials IMI (Boucherville, Québéc), and the Centre Quebécois de Recherche et Développement de l'Aluminium CQRDA (Chicoutimi, Québéc).

References

1. B. KULUNK, S. G. SHABESTARI, J. E. GRUZLESKI and D. J. ZULIANI: *AFS Trans.*, 1996, **104**, 1189–1193.
2. C. H. CACERES and B. I. SELLING: *Mater. Sci. Eng. A*, 1996, **220**, 109–116.
3. J. E. GRUZLESKI and B. CLOSSET: 'The treatment of liquid aluminum–silicon alloy', 155–157; 1990, Des Plaines, The American Foundrymen's Society.
4. J. M. BOILEAU, S. J. WEBER and R. H. SALZMAN: *AFS Trans.*, 2001, **109**, 419–432.
5. T. S. PIWONKA and M. C. FLEMINGS: *Trans. Metall. Soc. AIME*, 1966, **236**, 1157–1165.
6. D. E. J. TALBOT: *Int. Metall. Rev.*, 1975, **20**, 166–184.
7. W. MICHELS and S. ENGLER: *Giessereiforschung*, 1989, **41**, 174–187.
8. J. P. ANSON and J. E. GRUZLESKI: *AFS Trans.*, 2001, **109**, 243–258.
9. S. VISWANATHAN, V. K. SIKKA and H. D. BRODY: *JOM*, 1992, **Sept.**, 37–40.
10. V. K. SURI and A. J. PAUL: *AFS Trans.*, 1993, **101**, 949–954.
11. J. HUANG and J. G. CONLEY: *Rev. Prog. Quant. Nondestructive Evol.*, 1998, **17B**, 1839–1846.
12. A. S. SABAU and S. VISWANATAN: in 'Light metals 2000', 597–602; 2000.
13. D. R. POIRIER, P. K. SUNG and S. D. FELICELLI: *AFS Trans.*, 2001, **109**, 379–395.
14. W. H. JOHNSON and J. G. KURA: *AFS Trans.*, 1959, **67**, 532–552.
15. G. V. K. RAO and V. PANCHANATHAN: *AFS Trans.*, 1973, **88**, 110–114.
16. V. L. DAVIES: *AFS Cast Metals Res. J.*, 1975, **11**, 33–44.
17. E. NIYAMA and T. A. UCHIDA: *Int. Cast Metals J.*, 1982, **7**, 52–63.
18. Y. W. LEE, E. CHANG and C. F. CHIEU: *Metall. Trans. B*, 1990, **21B**, 715–722.
19. E. CHANG and Y. S. KUO: *AFS Trans.*, 1994, **102**, 167–172.
20. V. K. SURI, A. J. PAUL, N. EI-KADDAH and J. T. BERRY: *AFS Trans.*, 1994, **102**, 861–867.
21. V. K. SURI, C. CHENG, A. J. PAUL, N. EI-KADDAH and J. T. BERRY: in 'Light metals 1994', San Francisco, CA, USA; Feb–March 1994, 907–912.
22. S. T. KAO, E. CHANG and Y. W. LEE: *Mater. Sci. Technol.*, 1995, **11**, 933–938.
23. S. T. KAO and E. CHANG: *AFS Trans.*, 1996, **104**, 545–549.
24. Q. M. CHEN and C. RAVINDRAN: *AFS Trans.*, 2000, **108**, 279–305.
25. F. PARAY, J. CLEMENTS, B. KULUNK and J. E. GRUZLESKI: Proc. 35th Annual CIM Conference on 'Light metals', Montreal, Canada, August 1996, 666–675.
26. F. PARAY, J. CLEMENTS, B. KULUNK and J. E. GRUZLESKI: *AFS Trans.*, 1997, **105**, 791–801.
27. W. LA-ORCHAN, M. H. MULAZIMOGLU and J. E. GRUZLESKI: *AFS Trans.*, 1993, **101**, 253–259.
28. W. LA-ORCHAN: 'The quantification of the reduced pressure test', PhD thesis, McGill University, Montreal, Canada, Sept. 1994.
29. F. CHIESA and P. I. REGIMGAL: *AFS Trans.*, 2001, **109**, 347–357.
30. D. R. ANDERSON, D. J. SWEENEY and T. A. WILLIAMS: 'Statistics for business and Economics 8e', 551–556; 2001, Mason, South-Western (a division of Thomson Learning).